Review of Scientific Instruments

A 410 MHz resonant cavity pickup for heavy ion storage rings

Cite as: Rev. Sci. Instrum. **91**, 083303 (2020); https://doi.org/10.1063/5.0009094
Submitted: 27 March 2020 • Accepted: 09 August 2020 • Published Online: 28 August 2020

M. S. Sanjari, D. Dmytriiev, Yu. A. Litvinov, et al.

Review of Scientific Instruments ARTICLE scitation.org/journal/rsi

A 410 MHz resonant cavity pickup for heavy ion storage rings

Cite as: Rev. Sci. Instrum. 91, 083303 (2020); doi: 10.1063/5.0009094
Submitted: 27 March 2020 • Accepted: 9 August 2020 •
Published Online: 28 August 2020

M. S. Sanjari,[a] D. Dmytriiev,[b] Yu. A. Litvinov,[b] O. Gumenyuk,[c] R. Hess, R. Joseph, S. A. Litvinov, M. Steck, and Th. Stöhlker[d]

AFFILIATIONS

GSI Helmholtz Center for Heavy Ion Research, 64291 Darmstadt, Germany

[a]**Author to whom correspondence should be addressed:** s.sanjari@gsi.de
[b]**Also at:** Ruprecht Karls University, 69117 Heidelberg, Germany.
[c]**Present address:** CERN, 1211 Geneva, Switzerland.
[d]**Also at:** Helmholtz Institute, 07743 Jena, Germany and Friedrich Schiller University, 07743 Jena, Germany.

ABSTRACT

An improved design of a longitudinally sensitive resonant Schottky cavity pickup for the heavy ion storage rings of the Facility for Antiproton and Ion Research in Europe (FAIR) project is reported. The new detector has a higher measured Q value of ~3000 and a higher simulated shunt impedance of 473.3 kΩ. It is possible to vary the sensitivity of the cavity with a motorized mechanism by inserting a dissipative blade during the operation based on experimental needs. Apart from a lower price tag, the new design features a more robust and production-friendly mechanical structure suitable for a series production in the future FAIR project. The manufactured cavity was built temporarily into the experimental storage ring and had delivered its first results using stored heavy ion beams. The structure, simulation results, and performance of this cavity are presented in this work.

I. INTRODUCTION

Radio frequency (RF) cavities are used as pickups for non-destructive particle detection in storage rings. They have been standard tools in accelerator beam diagnostics for more than half a century. Longitudinal cavities provide information on beam revolution frequency and intensity. Their time resolved spectra can be used to gain information on the temporal change of the beam such as acceleration, deceleration, beam stacking, orbit shift, and cooling process, which can be utilized to optimize the related parameters. In combination with a radioactive ion beam (RIB) facility, the Schottky spectra of ions inside the storage ring can additionally be used for the precision determination of masses (Schottky mass spectroscopy) and lifetime of exotic nuclei. These quantities are essential for the study of nuclear structure and also play a significant role in the understanding of nucleosynthesis in the stars.[1–3]

In our previous work, we reported the successful design, manufacturing, and commissioning of a 245 MHz resonant Schottky cavity pickup for the experimental storage ring (ESR) at GSI Darmstadt.[4,5] This cavity was developed for the application of single particle decay spectroscopy in which radioactive decays of individually stored ions are detected.[6,7] Ever since, the cavity has played a prominent role in experiments involving the storage ring, during the setup, characterization, and also as the primary detector. Its functionality has been successfully demonstrated in several experiments.

Considerable experience had been gained using the 245 MHz resonant Schottky cavity pickup in previous years, and hence, many possible improvements for a follow-up design could be identified. In this work, a design upgrade is reported, which aims at addressing these improvements with regard to production for FAIR storage rings[8] as well as easier maintenance and setup. In comparison to the previous design, this work features a variable sensitivity, which can be applied during operation.

II. DESIGN AND CONSTRUCTION OF THE RESONANT PICKUP

A. Considerations for an improved design

1. The ceramic gap

We introduced the ceramic gap in the previous design[4] as a deliberate decision to protect the high intensity beams from loss of quality, such as unwanted bunching effects, due to the high impedance of the resonator. Furthermore, in order to facilitate the baking process of the ESR using a heating jacket at the place of the resonator, the two half shells of the resonator could be moved apart on a mechanical rail. After the heating process, the jackets could be removed and the two halves were fastened back together.

Ceramic gaps proved to be highly resource intensive and prone to mechanical irregularities that would affect their radio frequency (RF) properties. Since these RF properties were essential for the operation of the resonant Schottky cavity pickup, they had to be measured promptly after delivery using offline measurement setups. Some ceramic gaps had to be discarded, leading to immense losses in resources. The ceramic gap largely affected the Q value and hence the sensitivity of the previous 245 MHz cavity resonator, which was partly compensated by the copper coating of the interior part of the resonator and the plunger holders. The copper coating itself was a major resource intensive manufacturing step.

In the past few years, compared to the spectra from the ESR's parallel plate Schottky monitor[9] and the resonant Schottky cavity pickup, no bunching effects of the resonator were observed on high current heavy-ion beams inside the ESR. This was mainly due to its relatively moderate Q value and not so highly intense beams. As a result, the opening of the 245 MHz cavity resonator inside the ESR was never required. The effect on even higher current beams was not tested thoroughly due to the lack of such settings in beam time plan.

2. RF tightness

In order to provide RF tight connections between the two resonator body halves, and between the two halves and the ceramic gap, contact springs and elastic copper threads were used (cf. Fig. 3 of Ref. 4). After each maintenance phase in the ESR and the subsequent bake out, the resonator body halves have to be opened and closed. This process causes these contact springs and elastic copper threads to slowly wear out and lose their RF tightness. A full RF tightness could never be achieved, as a certain amount of RF leakage was measured using an external antenna in offline tests. Contact springs were also used for the plungers, which caused scratches on their surface.

3. Conclusion

For a storage ring such as an ESR with a diverse experimental program, a versatile cavity with movable parts indeed is the right choice for all future scenarios. The aim is to provide an improved design addressing the above issues with reproducible characteristics for installation in several storage rings, especially for storage rings of the Facility for Antiproton and Ion Research (FAIR).

B. Improvements

1. Cavity body

The primary design parameters were set with a straight section of the future Collector Ring (CR) in mind.[10] In order to avoid impedance steps, the same beam pipe size was used as in the straight section of the CR, i.e., 200 mm. In accordance with the mechanical restrictions of the section, the inner diameter of the cavity was chosen to be 594 mm, which results in the working frequency range of ~410 MHz. The inner depth was chosen to be small enough to minimize the transit time factor but large enough to avoid the distortion of the fields. The final value was set to 103 mm.

The ceramic gap was removed to allow for a fully evacuated resonator body. In order to avoid very high quality factors, the material of choice for the body and pipes was DIN 1.4404 (316L), for flanges DIN 1.4429 (316 LN ESU), and for support parts DIN 1.4301 (304) stainless steel. No copper coating was applied inside, making the design more suitable for the UHV cleaning and preparation. The body was milled out of a single piece, thereby reducing the welding paths in the most critical areas with highest surface currents to only one electron beam welded path, compared to many more in the previous design. In order to make sure that atmospheric pressure will not deform the evacuated body, numerical simulations were performed,[11] and hence, the thickness of the body was chosen to be 8 mm. Additional radial support blades were foreseen to enhance the stability in this regard.

Unlike the previous design, the present cavity is symmetric. This allows a better alignment of the field distribution in the fundamental (monopole TM010) mode with the mechanical axis. The symmetry in the design makes horizontal or vertical placement possible for offline lab use or for the storage ring installation and provides more stability during transport.

2. Plungers

Unlike the 245 MHz design, the plunger bodies are made of hollow stainless steel, hence reducing the weight for the motors. In the new design, smaller motor drive units and less mechanical parts have been used. No contact springs or elastic copper threads are needed as there are no moving parts except the plungers, which also do not utilize contact springs. Simulation results confirmed that the removal of the contact springs, although permitting field extension into the square ducts would cause insignificant change in the mode pattern, at most affects the eigenfrequency, which would be compensated by the plunger in any case. A heating jacket is permanently installed around the body of the resonator. Three small heating jackets for the bellows of the plungers are removed after the bake out. The heating jackets can be omitted for FAIR storage rings such as the Collector Ring (CR) for which UHV bake-out is not planned. The general structure of the cavity is shown in Fig. 1.

3. Variable sensitivity

Having a high quality factor is favorable for low intensity beams, but due to the narrow band nature of cavity resonators, beams of large momentum spread cannot be represented completely in the Schottky spectrum. Therefore, it is of practical advantage that the Q value and hence the sensitivity of the cavity could be varied during the operation in the storage ring.

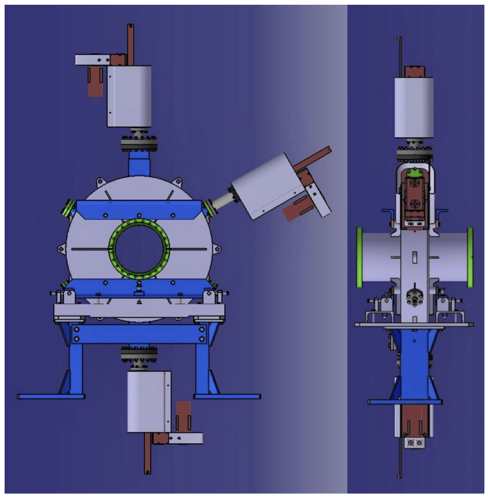

FIG. 1. The CAD design of the resonator: front view (left) and side view (right). The cavity is seen on its short support (blue) specially made for the ESR on top of an existing support. A stand-alone support structure has also been manufactured for the Collector Ring (CR) beam line. The frequency tuner plungers are situated on top and bottom. The detuner motor is seen on the side. Motors (red) are visible, whereas the bellows sections of the plunger drives are covered for protection.

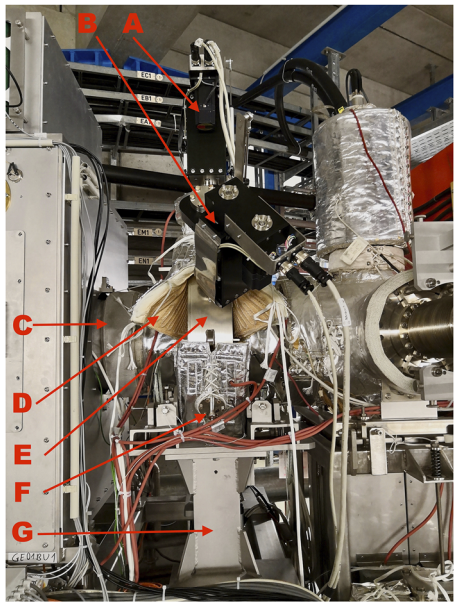

FIG. 2. Side view of the resonant cavity pickup in the ESR arc section on its support (compared with Fig. 1, right part). Visible components are (from top to bottom) (A) motor for the top tuner block; (B) motor for the detuner blade connected to port No. 4; (C) ESR beam tube; (D) heating jackets, which are pulled apart to expose the resonator body (E); (E) the resonator body; (F) port No. 3; and (G) mechanical support. Beam direction is from right to left (photograph: Sanjari, GSI Darmstadt, Germany, 2019).

Two different mechanisms have been implemented in order to vary the Q value and hence the sensitivity of the resonator. The first method involves motorized insertion of a dissipative blade into the cavity interior by means of a third stepper motor at the side (see Figs. 1 and 2), where the distribution of the magnetic monopole field is maximum at the rim of the resonator. Due to its small size and position, both the shunt impedance and the Q value will be reduced, thereby leaving the characteristic shunt impedance Ξ (refer to the definition in Sec. III A 2) nearly unchanged. In this work, a precisely machined sintered ferritic material TDK-IB-017 was used for the blade (dimensions 100 × 26 × 5 mm^3) whose UHV and bake-out properties were also tested separately and found to be in accordance with FAIR's UHV standards.[12] The second method of variable sensitivity utilizes a digital RF switch (Mini-Circuits MSP2TA-18-12BM+) in order to connect a 50 Ω resistive load to the over-coupled port, resulting in the change of the loaded Q [see Eq. (2)], allowing for a high and low state of Q value. While the first method can achieve values in between, the second method can additionally be used to switch between a high and low state. The two methods can be used simultaneously.

4. Ports

Three ports have been foreseen for magnetic loops. The couplers of two of the ports have been adjusted such that they roughly satisfy the critical condition (Nos. 2 and 3) by themselves and the coupler of the remaining port is adjusted to be highly over coupled (No. 1).

Couplers are constructed using large silver coated copper rectangular wire loops (area = 12 × 4 cm^2 and wire diameter 1.5 mm) on N-coaxial and bakeable vacuum feedthroughs. Port No. 4 is used for the blade driver.

5. Signal flow and processing

A low noise amplifier (Mini-Circuits ZX60-P103LN+) is connected to port No. 2 of the resonator. A bandpass filter (Minicircuits SXBP-404+), 15 m of low loss cable (Telegaertner 400 ZH G37), and a power amplifier (Mini-Circuits ZKL-1R5+) further process the signal before sending it across another 360 m of low loss cable (COFEED-0.5 in.) before the signal could be finally viewed and recorded on a real time spectrum analyzer (in our case, Tektronix RSA5103A) in the main control room (Fig. 3). The recorded

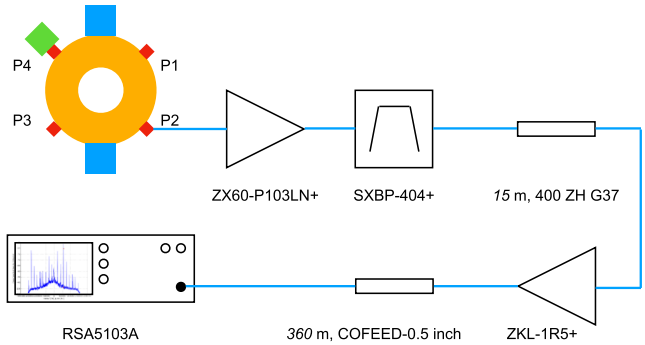

FIG. 3. The schematics of the RF signal flow showing the cavity (orange), tuner motors (blue), detune motor (green), ports (red), and different RF components and cables on the signal path. Port numbers are shown in the beam direction.

binary files are then processed offline using the IQTools Python library.[13,14]

III. RF PROPERTIES

A. Basic definitions

In order to estimate the sensitivity of the resonator using its offline measured properties, we recall some basic definitions in Secs. III A 1–III A 4.

1. Schottky signals

As particles pass through a region within a circular accelerator, they induce a periodic current on the walls of the beam tube. For fast particles, one can apply the *image current approximation*, which states that the induced image current is concentrated around a ring infinitely thin along the traveling direction of the charged particle. The resulting induced current $i(t)$ for a single particle would be a periodic delta function in time, while a collection of several of them constitute a particle distribution with different azimuthal phases.[15] Due to the random azimuthal phase offset of the particles around the ring, $i(t)$ is a random process whose expected value corresponds to the macroscopic DC beam current I_B, i.e., $\mathbb{E}[i(t)] = Zef_rN = I_B$, where N is the number of particles, e is the elementary charge, Z is the charge state, and f_r is the revolution frequency. The spectrum of this random process can be calculated using the Fourier transform of its *second order moment function*. This, in turn, shows peaks corresponding to every particle's revolution frequency, collectively known as *Schottky bands* around integer multiples of the revolution frequency h, while the peak width increases and peak height decreases with increasing harmonic number h. Nevertheless, the integral power remains the same for all bands while corresponding to half of the macroscopic DC current value I_B. The total noise power is then

$$\langle I \rangle^2 = 2(Ze)^2 f_r^2 N \tag{1}$$

in every band.[16]

2. Maximum allowable Q

Like any other resonant circuit, the resonant modes of the cavity can be characterized by three modal parameters: *frequency* f_0, *characteristic impedance* Ξ, and the *Q-value*. The cavity geometry can be designed to have a high excitation for a certain mode, i.e., a high characteristic impedance. The Q-value is a measure of how fast a cavity loses the stored energy[17,18] either due to the non-ideal surface resistance of the cavity material (known as unloaded Q or Q_0) or due to the external circuit, Q_{ext}. Loading results in an overall Q, called the loaded Q or Q_l,

$$\frac{1}{Q_l} = \frac{1}{Q_{ext}} + \frac{1}{Q_0}. \tag{2}$$

In other words, Q_l simply shows the effect of loading with resistor R_{ext}. If by adjusting the coupler, one can make sure that the same amount of power is lost in the walls as in the external circuit (this is known as *critical coupling*), then $Q_{ext} = Q_0$, which leads to a simplified form $Q_l = Q_0/2$, which, in turn, describes a nearly ideal transformer, allowing for the maximum power transfer with current ratio $I_{ext}/I_B = \sqrt{R_0/R_{ext}}$. At critical coupling, we also have $R_l = R_0/2$. The relation in Eq. (2) and the condition of critical coupling are valid only for a single coupler. Additional couplers on the same RF cavity will change the overall Q value depending on their loading condition, as given in Table II. The readout electronics is usually connected to a port that would allow an operation close to the critical condition depending on the desired loading setup on all ports. This is useful as a balance between achieving highest possible total Q_l and largest possible signal amplitude on the readout port.

For high Q resonators, the Q value can be measured using the frequency response curve,

$$Q = \frac{f_c}{B}, \tag{3}$$

where f_c is the center frequency and the B (bandwidth) is the full frequency width measured at half maximum power around the center frequency.[19]

The above-mentioned power that is lost to the mode is due to the mode's real valued impedance R_0 at resonance, averaged over one RF period. A quantity called *shunt impedance* can be defined such that $R_s = 2R_0$ as it is usually done in simulation codes and most literature. The (unloaded) characteristic impedance, here Ξ_0, is related to shunt impedance as

$$\Xi_0 = R_s/Q_0 = \hat{\Xi}_0 \Lambda(\beta)^2, \tag{4}$$

where Λ is the *transit time factor* as a function of relativistic β of the particle.[17] $\hat{\Xi}_0$ is the *frozen* characteristic impedance for the ideal case of an infinitely thin cavity and a particle traveling at the speed of light. The unloaded frozen characteristic impedance can be determined in bench-top measurements or by using the computer simulation code. The transit time factor can also be simulated (refer to Sec. III B). In the same manner for the loaded and external quantities, $\Xi_{ext} = R_{ext}/Q_{ext}$ and $\Xi_l = R_l/Q_l$.

For further analysis, the *phase slip factor* η needs to be considered, which is the relative slip in the revolution period T_r for an off-momentum particle in a storage ring. Thus,

$$\frac{\Delta f}{f_r} = \eta \frac{\Delta p}{p_r}, \tag{5}$$

where the subscript r denotes the revolution frequency around which the off-momentum particles with revolution frequencies f_1 and f_2 are located such that $\Delta f = f_2 - f_1$. The phase slip factor is related to the transition energy of the particle by $\eta = 1/\gamma_t^2 - 1/\gamma^2$, where $\gamma_t = \sqrt{1/\alpha}$ and α is the *momentum compaction factor*.[17] Hence, the phase slip factor may be positive or negative for a given optics setting due to α and particle energy. In the following, only the positive values of Δf are considered since we are dealing with the measurement of frequency bandwidths.

Equation (5) holds also for higher harmonics in Schottky bands, since both Δf and f scale with the harmonic number h. After tuning the resonator on top of a harmonic, i.e., $f_0 = hf_r$, using the tuner plungers, it should be reassured that $h\Delta f$ fits into the B of Eq. (3). An arbitrary factor a, which is larger than unity, can hence be multiplied, resulting in the maximum allowed Q value of a cavity in order for

any beam with given $\Delta p/p_r$ to be made completely visible by it. That is, with $B_{min} = ah\Delta f$, it could be concluded that

$$Q_{max} = \frac{hf_r}{B_{min}} = \frac{1}{a\eta\frac{\Delta p}{p_r}}. \quad (6)$$

In practical situations, the cavity bandwidth (and hence the factor a) should be much larger than the bandwidth of the beam distribution, which is a result of its temperature; otherwise, the measurement of momentum spread of the beam is distorted. For a beam with multiple or broad spectral components, the bandwidth should also be large enough to avoid the detection of particles at different frequencies with different sensitivities caused by the shape of the resonator frequency transfer function.

3. Signal power

Applying the conditions of critical coupling, we obtain $R_l = \frac{R_l}{Q_l}Q_l = \frac{1}{4}\hat{\Xi}_0\Lambda(\beta)^2Q_0$, which we then multiply with Eq. (1) to get the signal power,

$$\langle p\rangle = \frac{1}{2}(Ze)^2f_r^2N\hat{\Xi}_0\Lambda(\beta)^2Q_0. \quad (7)$$

As mentioned earlier, the total power remains the same in every band and ideally before and after the change in momentum spread. The measured value by a spectrum analyzer marker is therefore related to its resolution bandwidth RBW and Δf, i.e., marker value $= \frac{\mathrm{RBW}}{\Delta f}\langle p\rangle$, where Δf is the same as in Eq. (5).

4. Sensitivity and number of particles

Sensitivity, sometimes referred to as *minimum detectable signal* in the literature, is a signal with a power at the input of an RF system that produces an output signal to noise ratio of m, where m is, in practice, taken to be larger than unity, in order to make sure actual detection take place,[20]

$$S(dBm) = 10\log_{10}(kT_0\times 10^3) + 10\log_{10}(B) + F(dBm) + 10\log_{10}(m), \quad (8)$$

where $k = 1.38\times 10^{-23}$ J/K is the Boltzmann constant, T_0 is the temperature, and F is the logarithmic noise figure of the first amplifier stage, which is the largest contribution to signal to noise degradation.[21] At room temperature, the first term is the available noise power in mW for a bandwidth of 1 Hz, which is equivalent to −174 dBm. B is the analysis bandwidth in Hz. The maximum obvious value for B, as long as Schottky bands do not overlap, is $\pm f_r/2$, since anything beyond this range is the duplicated information from other harmonics. However, $h\Delta f$ is used here in order to have equal noise and signal bandwidth in the calculation around harmonic h.

In order to get the minimum number of particles needed to create a strong enough signal visible out of the noise background with the given signal-to-noise ratio (SNR) of m, we rearrange Eq. (7) and put the minimum detectable signal from Eq. (8) as its required total power,

$$N_{min} = \frac{2S(W)}{(Ze)^2f_r^2\hat{\Xi}_0\Lambda(\beta)^2Q_0}, \quad (9)$$

where $S(W)$ is $S(dBm)$ converted to units of Watt.

TABLE I. Simulated modes of the cavity. The conductivity of the 316 stainless steel was assumed to be 1.33×10^6 S/m. Losses are normalized to 1 J stored energy and include surface and volume losses.

Mode name	Freq. (MHz)	Q	Power lost in mode (W)
TM_{010}	405.81	2796	9.10×10^5
TM_{110}	580.56	3443	1.05×10^6
TM_{110} (rotated)	582.80	2407	1.52×10^6
TM_{210}	806.93	3099	1.64×10^6
TM_{210} (rotated)	810.69	1694	3.00×10^6
TM_{020}	939.55	1790	3.29×10^6
TM_{310}	1013.51	1129	5.64×10^6
TM_{310} (rotated)	1020.85	5640	1.14×10^6

B. Simulation results

Field simulations have been performed using the CST Studio Suite.[22] The major modes below the cutoff frequency of the beam pipe (~880 MHz) are summarized in Table I. It can be seen that the rotated dipole mode has a slightly higher frequency due to the

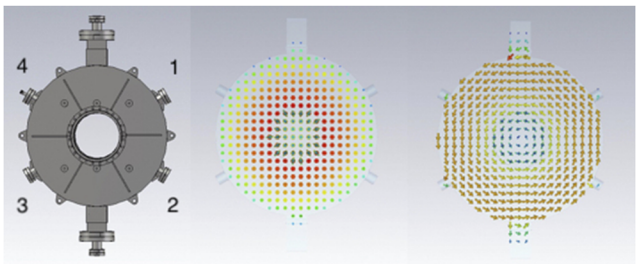

FIG. 4. Numeric simulation of the electromagnetic fields and impedance of the fundamental oscillation mode. The CAD model (left), electric field arrows (middle), and magnetic field arrows (right). Port numbers are shown in the beam direction.

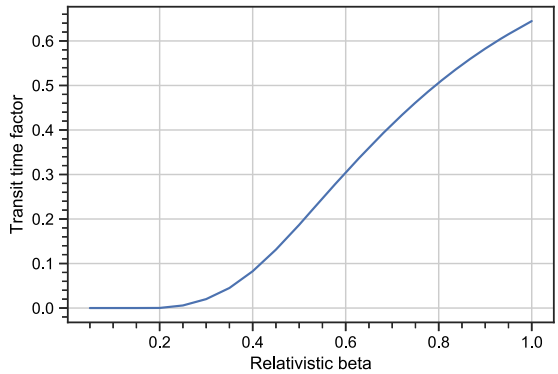

FIG. 5. Simulated transit time factor of the cavity for the fundamental monopole mode at the geometric center and for different relativistic beta values in 0.05 steps.

larger openings for the plungers. The distribution of the electric and magnetic field components is shown in Fig. 4.

The resulting frozen characteristic impedance of the fundamental monopole mode that is maximum at the geometric center is $\hat{\Xi}_0 = 136.35\ \Omega$ and the shunt impedance $R_s = 473.3\ \text{k}\Omega$. At the same location, the transit time factor was simulated for different relativistic beta values and is shown in Fig. 5.

IV. MEASURED PERFORMANCE

A. Offline measurements

1. Frequency, Q value, and port coupling constant

Changing the boundary conditions of cavity resonators changes their characteristic frequency.[23,24] The plungers are moved simultaneously in order to make sure that the electrical and geometrical centers remain close to each other. While the main goal of the plungers is to change the tuning frequency, other quantities change slightly as a result and need to be measured as well. The Q value was measured using s-parameters in reflection.[18,25] The coupling constant is then calculated from the loaded and unloaded Q using Eq. (2). Figure 6 shows the measurement results.[26] The tuning frequency range is relatively linear within the first 60 mm. It can be seen that apart from a large discontinuity afterward, which can be related to a dominant excitation of a higher order mode, Q values and port coupling constants are relatively stable around their design value, i.e., port Nos. 2 and 3 roughly satisfy the critical condition and port No. 1 is largely over-coupled. Furthermore, the scattering might be attributed to the significant sensitivity of the coupling constants on the tightening of the flanges of the corresponding couplers.

For the next measurement, the detuner blade is moved inside the cavity, while its broad side is facing the beam line. The advantage of the detuning cavity using this method is the reduction in Q_0, which is well achieved and it is shown in Fig. 7. A slight change in frequency is visible as well.

Another common technique to reduce the Q value utilizes loading one of the free ports. In order to achieve the optimized and precise values of Q, methods using matched transmission lines and stubs can be used, as found in the literature.[27] For a quick reduction in the Q value, a 50 Ω load is switched onto the over-coupled ports, while the readout remains connected to port No. 2. This results in different high-Q and low-Q states as given in Table II. The combination of the resistive loading is possible with all different positions of the blade. For simplicity, only the extreme values are shown in this table, where the blade is either fully retracted or fully inside the cavity.

2. Estimation of sensitivity

Using the measured values from Fig. 7, the sensitivity of the cavity pickup can be estimated. In the approximate region of critical coupling, $Q_0 \sim 3000$ at $f_0 = 407.24$ MHz. At this frequency, the LNA has a noise figure $F = 0.77$ dB.[28] The ESR has a circumference of 108.4 m with a typical $\gamma_t = 2.3$ in the standard mode of operation.

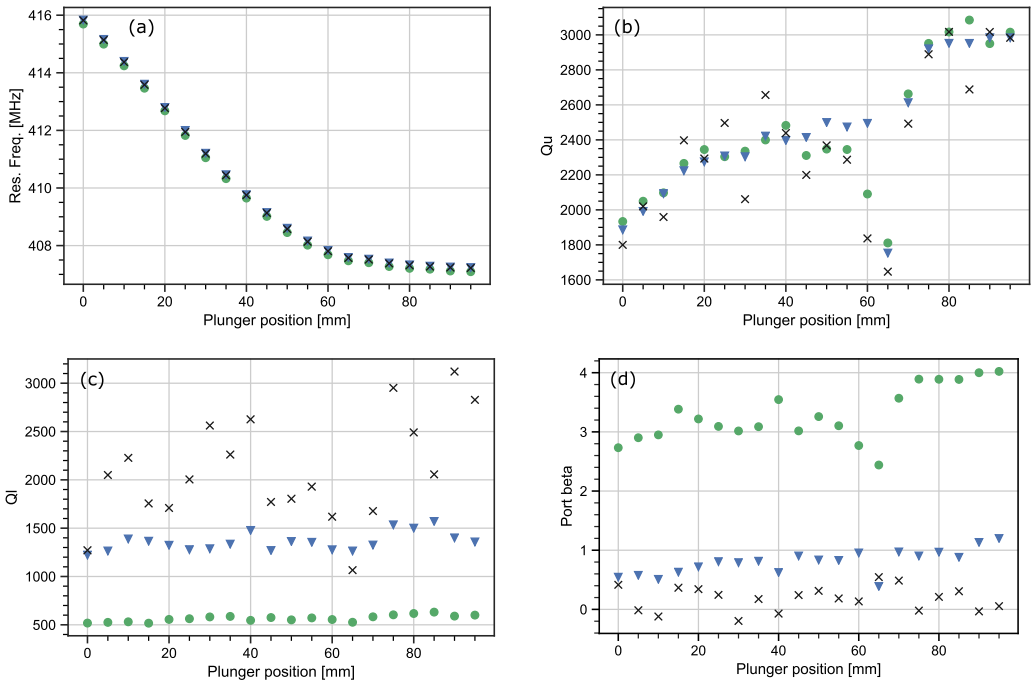

FIG. 6. Resonance frequency of the monopole mode f_0 (a), Q_0 (b), Q_l (c), and coupling constant β (d) measured from port No. 1 (dots), port No. 2 (triangles), and port No. 3 (crosses) at different plunger positions (zero means fully inside, i.e., closest to the beam axis), while the blade is fully outside. Both plungers move simultaneously. Each point is the result of an average of 10 consecutive measurements.

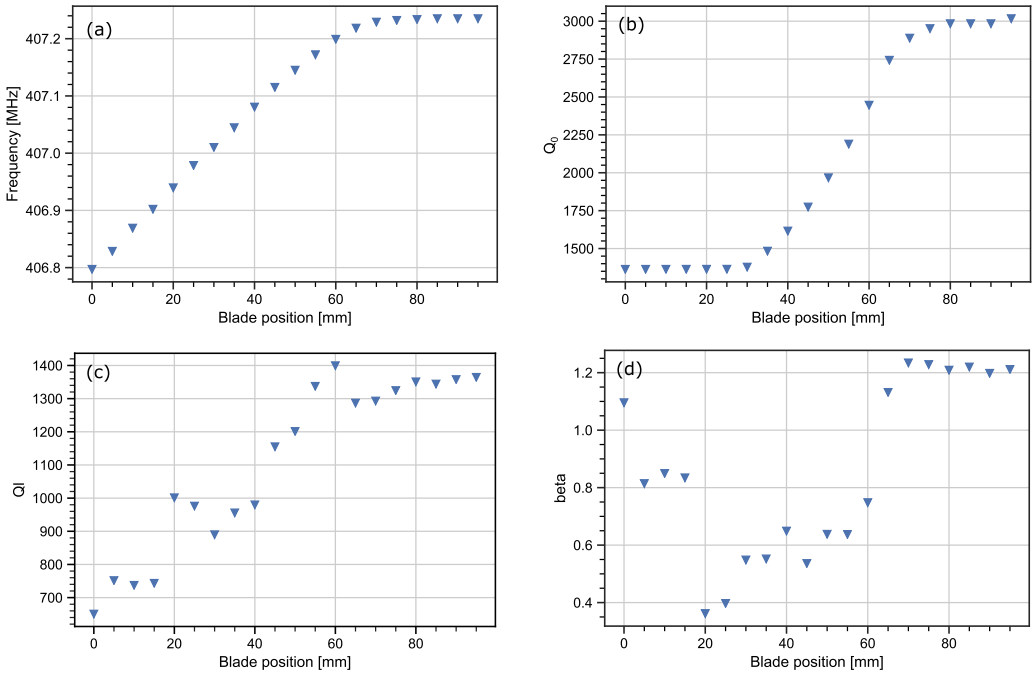

FIG. 7. Resonance frequency of the monopole mode f_0 (a), Q_0 (b), Q_l (c), and coupling constant β (d) measured from port No. 2 (triangles) at different blade positions (zero means fully inside, i.e., closest to the beam axis), while both plungers are fully outside. Each point is the result of an average of 10 consecutive measurements.

Assuming a moderately cooled beam with $\Delta p/p \sim 10^{-5}$ at 400 MeV/u, we obtain f_r, relativistic γ and β, η (using Fig. 5), $\Lambda(\beta)$, and h. The condition of Eq. (6) is satisfied with $a \gg 1$. If now a signal-to-noise ratio of $m = 2$ is required, then with $S(dBm) \sim -139.31$, it can be seen that according to Eq. (8), single particle sensitivity is expected already at charge states around or less than 60. At 350 MeV/u, this value is ~66 and at 300 MeV/u, 81. These estimates are in accordance with our experience with the previous resonator.[6,7] In practical cases, the sensitivity will be higher when combined with spectral estimation methods and averaging.

B. Online measurements

The cavity pickup could be tested during the machine test beam time in April and November 2019 allowing for several minutes of recording time for different beam types. Figure 8 shows a qualitative comparison of the dynamic loading method: a 1.25 mA beam of 232 MeV/u $^{107}Ag^{45+}$ is cooled down using ESR's electron cooler. The diagram shows the power spectrum (color) vs time (vertical, from top to bottom) vs frequency (horizontal) axis.

Figure 9 shows how the position of the blade can be used to decrease the Q value of the cavity and hence the sensitivity by inserting it in, as compared to when it is taken out (right side of the diagram). The blade (and plungers) can be moved anytime during the injection cycle with a speed of 3 mm/s. These results are in accordance with the offline measurement results presented in Table II.

The ESR is fully packed with experimental devices and chambers. Due to the lack of space in the straight section of the ring, which is preferable for the installation of the longitudinal cavity pickups

TABLE II. Measured quantities at port No. 2 while using a 50 Ω load on port Nos. 1, 3, none, or both at two states of the blade position.

	Blade fully outside				Blade fully inside			
Load connected to	None	P1	P3	P1 and P3	None	P1	P3	P1 and P3
Unloaded Q	3017	1364	1371	1364	1363	1362	1363	1362
Loaded Q	1351	621	908	367	649	373	634	372
Freq. (MHz)	407.2	407.2	407.2	407.2	406.8	406.7	406.8	406.7
Coupl. factor	1.2	1.2	0.5	2.7	1.1	2.7	1.2	2.7

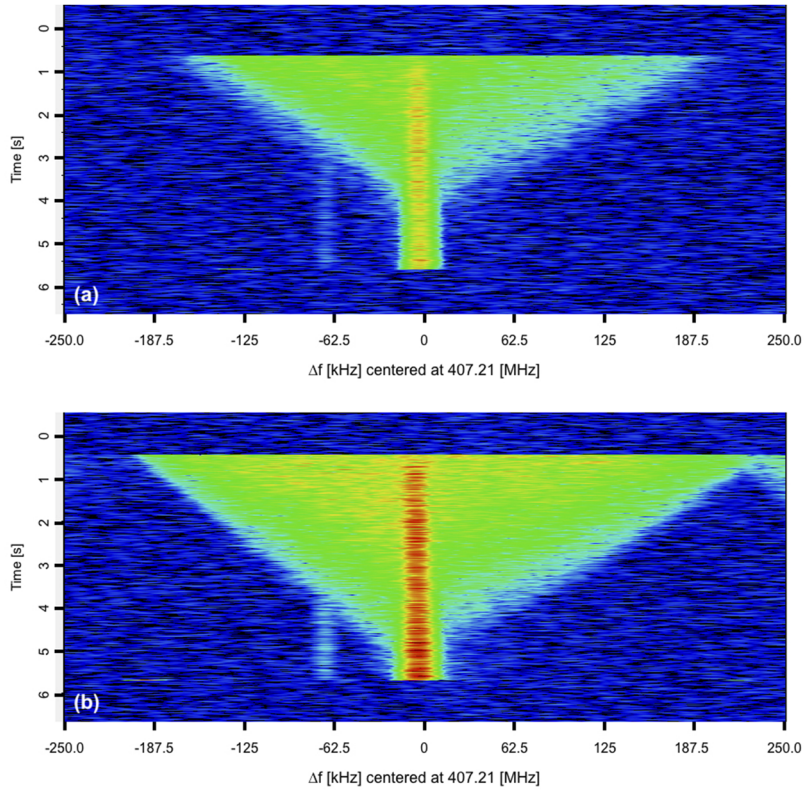

FIG. 8. Electron cooling of a 1.25 mA, 232 MeV/u $^{107}Ag^{45+}$ beam in (a) low Q state (all plungers out, 50 Ω on the over-coupled port) and (b) high Q states (all plungers out, 50 Ω on the over-coupled port), showed with a span of 500 kHz. The 245th harmonic is centered at 407.21 MHz. Time ticks are in seconds, continuously running from top to bottom.

due to low dispersion, a section in the arc was chosen as the test location. Due to high horizontal dispersion at this location, the spectra show additional sidebands as a result of the betatron motion of the particles. An example of such a sideband is shown in Fig. 10. These sidebands appear on both sides of the main peak with frequency deviations much less than the revolution frequency. In the specific case of Fig. 10, only the left sideband is visible, since the f_0 of the resonator is not exactly corresponding to the frequency of the stored beam, but rather to the left of it, allowing for enough sensitivity to

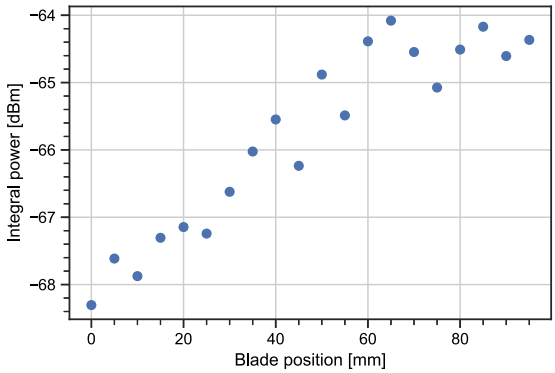

FIG. 9. Measurement of the peak power of an $^{40}Ar^{18+}$ beam at 250 MeV/u containing 1.2×10^8 particles at different blade positions (zero means fully inside, i.e., closest to the beam axis), while both plungers are fully outside. Each point represents the time average of 400 consecutive frames (each frame containing 2^{13} FFT points with a length of 5.24 ms) of an ~2 s of recorded data at 407.88 MHz.

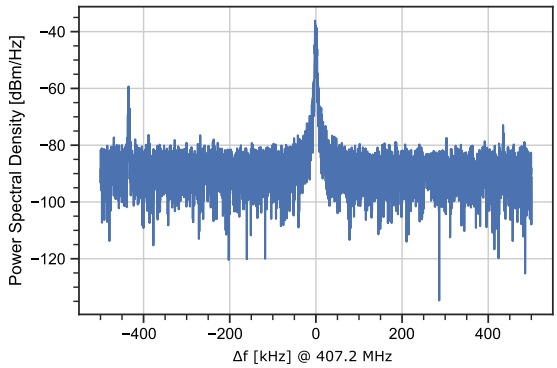

FIG. 10. A spectrum of the beam showing the main peak and two betatron sidebands at ±435 kHz. Beam and spectrum parameters are the same as in Fig. 9. The blade and both plungers are fully retracted outside. This shifts the resonant frequency of the cavity to the minimum possible value around 407 MHz [compared with Fig. 6(a)]. At this frequency, the cavity has its highest impedance possible. The impedance falls off on both sides so that the right sideband is shorter than the left sideband because it is further away from the resonance center (~600 kHz for the right sideband vs ~200 kHz for the left sideband).

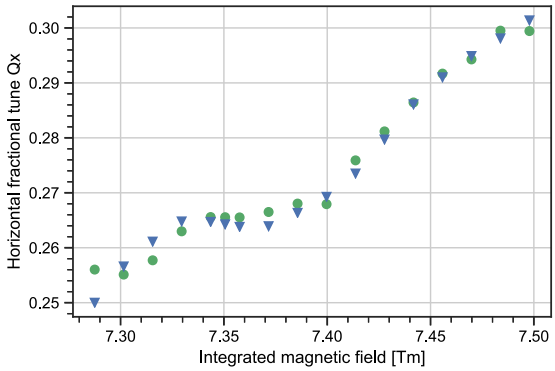

FIG. 11. Measurement of the horizontal tune of the ESR while changing the magnetic field of the main ESR dipole with a 330 MeV/u $^{107}Ag^{43+}$ beam using the conventional method of the beam transfer function (dots) and using the longitudinal resonant cavity (triangles). Each point represents the time average of 10 consecutive spectra.

capture the left sideband, but not the right sideband. Schottky analysis for mass and lifetime measurements is usually not done at such large bandwidths. Nevertheless, these sidebands can be used to measure the horizontal tune of the ESR in this specific setup by dividing the deviation from the main peak by the revolution frequency. The result is shown in Fig. 11. Here, the energy of the beam has been kept constant, while the optics have been changed.

V. CONCLUSION AND OUTLOOK

In this work, an upgraded design of a longitudinally sensitive resonant Schottky cavity pickup for heavy ion storage rings at the FAIR is introduced. It features more robust mechanical features, fewer number of mechanical parts compared to the previous design, easier construction, and a variable sensitivity mechanism that can be used during the operation as a part of the accelerator beam cycle.

Due to the reduced operation of GSI accelerators, the single particle sensitivity could not be tested, although it is expected, as described in Sec. IV A. Single-particle sensitivity is the major goal for the development of such detectors for the FAIR. Therefore, it will be thoroughly addressed and reported in a future contribution.

It is possible to reduce the Q factor even further using the matched transmission line and stubs, as mentioned earlier. This can be done without any interruption in the vacuum installation, since port properties are very well measured.

As mentioned earlier, the temporary installation location of the cavity pickup in the ESR in a highly dispersive region gives rise to effects, which make further investigation of the coupling mechanism to a purely longitudinal pickup interesting. This is specifically important, since in the future FAIR project, the collector ring (CR) will utilize longitudinal cavities in its dispersive section as well.[29]

ACKNOWLEDGMENTS

We would like to thank F. Caspers (CERN) for fruitful discussions. We are indebted to our GSI colleagues for help during various stages of the construction and commissioning of the cavity: D. Acker, M. C. Bellachioma, M. Bevcic, J. Bönsch, R. Boywitt, J. Cavaco Da Silva, K. Dermati, H. E. Durand-Paredes, Z. Fekete, R. Fischer, J. Holluba, K. Kalaitzidis, E. Keller, Ch. Kolligs, Ch. Kozhuharov, S. Kredel, J. Kurdal, B. A. Lorentz, S. Matthies, F. Nolden, N. Petridis, E. Renz, M. Rosan, M. Romig, G. Savino, T. Schneider, I. Schurig, S. Schuhmacher, W. Sturm, M. P. Suherman, S. Teich, L. Urban, R. Vincelli, O. Zurkan, and the ILIMA and SPARC collaborations. Finally, we would also like to thank J. Häuser (Kress GmbH).

This project has received funding from the European Research Council (ERC) under the European Union's Horizon 2020 research and innovation program (Grant Agreement No. 682841 "ASTRUm"). D.D. acknowledges support from the HGS-HIRe and Heidelberg Graduate School for Physics (HGFSP).

DATA AVAILABILITY

The data that support the findings of this study are available from the corresponding author upon reasonable request.

REFERENCES

[1] Y. A. Litvinov and F. Bosch, "Beta decay of highly charged ions," Rep. Prog. Phys. **74**, 016301 (2010).
[2] F. Bosch and Y. A. Litvinov, "Mass and lifetime measurements at the experimental storage ring of GSI," Int. J. Mass Spectrom. **349-350**, 151–161 (2013).
[3] F. Bosch, Y. A. Litvinov, and T. Stöhlker, "Nuclear physics with unstable ions at storage rings," Prog. Part. Nucl. Phys. **73**, 84–140 (2013).
[4] F. Nolden, P. Hülsmann, Y. A. Litvinov, P. Moritz, C. Peschke, P. Petri, M. S. Sanjari, M. Steck, H. Weick, J. X. Wu, Y. D. Zang, S. H. Zhang, and T. C. Zhao, "A fast and sensitive resonant Schottky pick-up for heavy ion storage rings," Nucl. Instrum. Methods Phys. Res., Sect. A **659**, 69–77 (2011).
[5] M. S. Sanjari, "Resonant pickups for non-destructive single-particle detection in heavy-ion storage rings and first experimental results," Ph.D. thesis, Johann Wolfgang Goethe-Universität, Frankfurt am Main, 2013.
[6] P. Kienle, F. Bosch, P. Bühler, T. Faestermann, Y. A. Litvinov, N. Winckler, M. S. Sanjari, D. B. Shubina, D. Atanasov, H. Geissel, V. Ivanova, X. L. Yan, D. Boutin, C. Brandau, I. Dillmann, C. Dimopoulou, R. Hess, P. M. Hillebrand, T. Izumikawa, R. Knöbel, J. Kurcewicz, N. Kuzminchuk, M. Lestinsky, S. A. Litvinov, X. W. Ma, L. Maier, M. Mazzocco, I. Mukha, C. Nociforo, F. Nolden, C. Scheidenberger, U. Spillmann, M. Steck, T. Stöhlker, B. H. Sun, F. Suzaki, T. Suzuki, S. Y. Torilov, M. Trassinelli, X. L. Tu, M. Wang, H. Weick, D. F. A. Winters, N. Winters, P. J. Woods, T. Yamaguchi, G. L. Zhang, and T. Ohtsubo, "High-resolution measurement of the time-modulated orbital electron capture and of the β+ decay of hydrogen-like 142Pm60+ ions," Phys. Lett. B **726**, 638–645 (2013).
[7] F. C. Ozturk, B. Akkus, D. Atanasov, H. Beyer, F. Bosch, D. Boutin, C. Brandau, P. Bühler, R. B. Cakirli, R. J. Chen, W. D. Chen, X. C. Chen, I. Dillmann, C. Dimopoulou, W. Enders, H. G. Essel, T. Faestermann, O. Forstner, B. S. Gao, H. Geissel, R. Gernhäuser, R. E. Grisenti, A. Gumberidze, S. Hagmann, T. Heftrich, M. Heil, M. O. Herdrich, P.-M. Hillenbrand, T. Izumikawa, P. Kienle, C. Klaushofer, C. Kleffner, C. Kozhuharov, R. K. Knöbel, O. Kovalenko, S. Kreim, T. Kühl, C. Lederer-Woods, M. Lestinsky, S. A. Litvinov, Y. A. Litvinov, Z. Liu, X. W. Ma, L. Maier, B. Mei, H. Miura, I. Mukha, A. Najafi, D. Nagae, T. Nishimura, C. Nociforo, F. Nolden, T. Ohtsubo, Y. Oktem, S. Omika, A. Ozawa, N. Petridis, J. Piotrowski, R. Reifarth, J. Rossbach, R. Sánchez, M. S. Sanjari, C. Scheidenberger, R. S. Sidhu, H. Simon, U. Spillmann, M. Steck, T. Stöhlker, B. H. Sun, L. A. Susam, F. Suzaki, T. Suzuki, S. Y. Torilov, C. Trageser, M. Trassinelli, S. Trotsenko, X. L. Tu, P. M. Walker, M. Wang, G. Weber, H. Weick, N. Winckler, D. F. A. Winters, P. J. Woods, T. Yamaguchi, X. D. Xu, X. L. Yan, J. C. Yang, Y. J. Yuan, Y. H. Zhang, and X. H. Zhou, "New test of modulated electron capture decay of hydrogen-like 142Pm ions: Precision measurement of purely exponential decay," Phys. Lett. B **797**, 134800 (2019).

[8]M. Steck, C. Dimopoulou, A. Dolinskii, O. Gorda, V. Gostishchev, K. Knie, S. Litvinov, F. Nolden, C. Peschke, and D. Obradors-Campos, "Status of the design of the fair storage rings," Int. J. Mod. Phys. E **18**, 411–419 (2009).
[9]U. Schaaf, "Schottky-diagnose und BTF-messungen an gekühlten strahlen im schwerionen-speicherring ESR," Ph.D. thesis, Johann Wolfgang Goethe-Universität, Frankfurt am Main, 1991.
[10]Collector Ring Working Group, "Technical design report collector ring," Technical Design Report No. 1608518, GSI Darmstadt, 2014.
[11]K. Dermati, "FEM analysis and simulation of Schottky resonator. Distribution of mechanical strength and deformation during vacuum load," GSI Darmstadt, 2015.
[12]C. Bellachioma, J. Cavaco, C. Kolligs, and M. P. Suherman, "Vacuum acceptance test F-PP-VC-EXP-0003," Technical Report No. F-PP-VC-EXP-0003, GSI Darmstadt, 2018.
[13]M. S. Sanjari, C. Kleffner, and Y. A. Litvinov, "Python code for Schottky analysis in storage ring experiments," GSI Scientific Report 2015, FG-GENERAL-19, 2016, p. 234.
[14]See https://github.com/xaratustrah/iqtools for the open source python library can be found at M. S. Sanjari, IQTools Library, 2019.
[15]S. Chattopadhyay, "Some fundamental aspects of fluctuations and coherence in charged-particle beams in storage rings," CERN-84-11, 1984; available at http://cds.cern.ch/record/155458.
[16]F. Caspers, "Schottky signals for longitudinal and transverse bunched-beam diagnostics," CERN Doc. Server (published online, 2008).
[17]A. W. Chao, K. H. Mess, M. Tigner, and F. Zimmermann, *Handbook of Accelerator Physics and Engineering* (World Scientific, 2013).
[18]E. L. Ginzton, *Microwave Measurements*, International Series on Pure and Applied Physics (McGraw-Hill, 1957).
[19]R. E. Collin, *Foundations for Microwave Engineering*, 2nd ed. (Wiley-IEEE Press, 2000).
[20]Agilent Technologies, "Fundamentals of RF and microwave noise figure measurements," Application Note 57-1, 2010.
[21]H. T. Friis, "Noise figures of radio receivers," Proc. IRE **32**, 419–422 (1944).
[22]See https://www.3ds.com/products-services/simulia/products/cst-studio-suite/ for the information page on the used imulation code.
[23]J. Müller, "Untersuchungen über elektromagnetische hohlräume," Z. Elektrotech. **54**, 157–161 (1939).
[24]L. C. Maier, Jr. and J. C. Slater, "Field strength measurements in resonant cavities," J. Appl. Phys. **23**, 68–77 (1952).
[25]F. Caspers, "RF engineering basic concepts: The Smith chart," CERN Doc. Server **2010**, 95–116.
[26]See https://github.com/xaratustrah/sparameter for the evaluation process.
[27]W. Schminke, "Strong damping of single-cell accelerator cavities by resonant loops," CERN Doc. Server (published online, 1981); available at https://cds.cern.ch/record/999483.
[28]C. Peschke, "Noise figure measurement of ZX60-P103LN+ low noise amplifiers," GSI Darmstadt, 2018.
[29]M. S. Sanjari, Y. A. Litvinov, and C. Kozhuharov, "Technical report for the design, construction and commissioning of the Schottky detector system for ILIMA," Technical Design Report No. FAIR-000006136, GSI Darmstadt, 2018.